Author/s:
Farmer, DGS;Pracejus, N;Dempsey, B;Turner, A;Bokiniec, P;Paton, JFR;Pickering, AE;Burguet, J;Andrey, P;Goodchild, AK;McAllen, RM;McMullan, S

Title:
On the presence and functional significance of sympathetic premotor neurons with collateralized spinal axons in the rat

Date:
2019-07-01

Citation:
Farmer, D. G. S., Pracejus, N., Dempsey, B., Turner, A., Bokiniec, P., Paton, J. F. R., Pickering, A. E., Burguet, J., Andrey, P., Goodchild, A. K., McAllen, R. M. & McMullan, S. (2019). On the presence and functional significance of sympathetic premotor neurons with collateralized spinal axons in the rat. Journal of Physiology, 597 (13), pp.3407-3423. https://doi.org/10.1113/JP277661.

DOI: 10.1113/JP277661

On the presence and functional significance of sympathetic premotor neurons with collateralised spinal axons in the rat

David G.S. Farmer[1]*, Natasha Pracejus[1]*, Bowen Dempsey[2], Anita Turner[3], Phillip Bokiniec[4], Julian F.R. Paton[5], Anthony E. Pickering[6], Jasmine Burguet[7], Phillipe Andrey[7], Ann K. Goodchild[3], Robin M. McAllen[1], and Simon McMullan[3]

* Indicates joint authorship.

[1]Florey Institute of Neuroscience and Mental Health, University of Melbourne, Victoria, 3052, Australia

[2]Neuroscience Paris-Saclay Institute (Neuro-PSI), CNRS, 91190 Gif-Sur-Yvette - France

[3]Faculty of Medicine & Health Science, Macquarie University, NSW 2109, Australia

[4]Department of Neuroscience, Max Delbrück Center for Molecular Medicine (MDC), Berlin-Buch, Germany; Neuroscience Research Center and Cluster of Excellence NeuroCure, Charité-Universitätsmedizin, Berlin, Germany.

[5]Department of Physiology, Faculty of Medical & Health Sciences, University of Auckland, Park Road, Grafton, Auckland 1142, New Zealand

[6]School of Physiology, Pharmacology & Neuroscience, Biomedical Sciences, University of Bristol, Bristol BS8 1TD, U.K.

[7] Institut Jean-Pierre Bourgin, INRA, AgroParisTech, CNRS, Université Paris-Saclay, 78000, Versailles, France

Correspondence

Robin McAllen
Florey Institute of Neuroscience and Mental Health
University of Melbourne
Parkville, Vic 3010
Australia

Email: rmca@florey.edu.au

Key Points

- Spinally-projecting neurons of the rostral ventrolateral medulla (RVLM) determine sympathetic outflow to different territories of the body.
- Previous studies suggest the existence of RVLM neurons with distinct functional classes: i.e. neurons that target sympathetic nerves bound for functionally-similar tissue types (e.g. muscle vasculature). The existence of RVLM neurons with more general actions had not been critically tested.
- Using viral tracing we show that a significant minority of RVLM neurons send axon collaterals to disparate spinal segments (T_2 and T_{10}).
- Furthermore, optogenetic activation of sympathetic premotor neurons that project to lumbar spinal segments also produced activation of sympathetic nerves from rostral spinal segments that innervate functionally diverse tissues (heart and forelimb muscle).
- These findings suggest the existence of individual RVLM neurons whose axons branch to drive sympathetic preganglionic neurons of more than one functional class and may be able to produce global changes in sympathetic activity.

Abstract

Here we investigate the extent of spinal axon collateralization of rat RVLM sympathetic premotor neurons and its functional consequences. In anatomical tracing experiments, two recombinant herpes viral vectors with retrograde tropism and expressing different fluorophores were injected into the intermediolateral column at upper thoracic and lower thoracic levels. Histological analysis revealed that ~21% of RVLM bulbospinal neurons were retrogradely labelled by both vectors, indicating substantial axonal collateralisation to disparate spinal segments. In functional experiments, another virus with retrograde tropism, a canine adenovirus expressing Cre recombinase, was injected into the left intermediolateral horn around the thoracolumbar junction, while a Cre-dependent viral vector encoding Channelrhodopsin2 under LoxP control was injected into the ipsilateral RVLM. In subsequent terminal experiments blue laser light (473nm x 20 ms pulses at 10 mW) was used to activate RVLM neurons that had been transduced by both vectors. Stimulus-locked activation, at appropriate latencies, was recorded in the following pairs of sympathetic nerves: forelimb and hindlimb muscle sympathetic fibres; cardiac and either hindlimb muscle or lumbar sympathetic nerves. The latter result demonstrates that axon collaterals of lumbar-projecting RVLM neurons project to, and excite, both functionally similar (forelimb and hindlimb muscle) and functionally dissimilar (lumbar and cardiac) preganglionic neurons. Together, these findings show that the axons of a significant proportion of RVLM neurons collateralise widely within the spinal cord, and that they may excite preganglionic neurons of more than one functional class.

Abbreviations:

Rostral ventrolateral medulla	RVLM
Muscle vasoconstrictor	MVC

1 Introduction

The rostral ventrolateral medulla (RVLM) contains spinally projecting neurons that monosynaptically innervate sympathetic preganglionic neurons and are a major supply of the essential tonic drive that maintains arterial blood pressure (reviewed by Dampney, 1994; Guyenet, 2006).When activated experimentally, these neurons raise blood pressure and excite sympathetic nerves innvervating a range of organs and tissues (Dampney & McAllen, 1988; McAllen & May, 1994; Abbott *et al.*, 2009), but do not appear to drive 'non-cardiovascular' sympathetic classes such as sudomotor, pilomotor, pupillodilator, brown adipose thermogenic, or intestinal motility inhibitory neurons (McAllen, 1986; Cao *et al.*, 2010).

While the cardiovascular actions of RVLM premotor neurons are not in doubt, there is evidence of functional heterogeneity within this population. In cat, localized nanoinjections of excitatory amino acids into different subregions of the RVLM were found to preferentially or exclusively activate vasomotor sympathetic nerves to different tissues (Dampney & McAllen, 1988; McAllen & Dampney, 1990; McAllen & May, 1994). McAllen and Dampney (1990) found that vasoconstrictor nerves to forelimb and hindlimb muscles were coactivated independently from renal sympathetic nerves, and concluded that RVLM subregions were most likely organised topographically by the function, rather than the anatomical location, of their peripheral vascular targets. Although the limited spatial resolution of the method makes the functional separation of these outputs more difficult in the rat, it has been demonstrated that sympathetic outflows of different functional classes are activated to varying degrees by RVLM nanoinjections in this species too (Beluli & Weaver, 1991a, b; Mueller *et al.*, 2011).

In addition to the above evidence for central topography based on function, individual RVLM neurons have also been found to display heterogeneous functional properties. For example, there are differences in their sensitivities to stimulation of arterial baroreceptors or somatic nerves (McMullan *et al.*, 2008; Verberne & Sartor, 2010), and to central respiratory drive (McAllen, 1987; Miyawaki *et al.*, 1995; Moraes *et al.*, 2013). Corresponding diversity is found among different peripheral sympathetic nerve classes (Janig & McLachlan, 1992) and indeed in the properties of the sympathetic preganglionic neurons (Morrison & Cao, 2000; Stalbovskiy *et al.*, 2014). One particularly clear example is the sympathetic control of adrenaline secretion, which seems to be controlled by a group of atypical RVLM bulbospinal neurons that are insensitive to baroreceptor stimulation but are activated by glucoprivation (Verberne & Sartor, 2010). These cells may selectively drive adrenal nerve activity, and therefore adrenaline secretion, in response to hypoglycaemic stimuli (Korim *et al.*, 2014; Korim *et al.*, 2016).

The two lines of evidence noted above lead naturally to the hypothesis that individual RVLM neurons are functionally dedicated to drive a single class of peripheral sympathetic neuron (e.g. muscle vasoconstrictor or cardioaccelerator). Against this notion is the general observation that RVLM nanoinjections nearly always co-activate more than one peripheral sympathetic neuron class (Beluli & Weaver, 1991b). Whilst this finding might be explained by the spatial spread of nanoinjected substances, no experiment has yet excluded the alternative possibility that there are also 'generalist' RVLM neurons with descending connections that synapse with more than one functional class of sympathetic outflow. The discovery of such neurons would suggest that an earlier view of the sympathetic nervous system, that of a monolithic and global effector system that "seem[s] devised for widespread diffusion of nervous impulses"; should be reconsidered (Cannon, 1915).

If 'generalist' RVLM neurons exist, one might predict that their descending axons branch to innervate preganglionic neurons of a range of functional classes at multiple spinal segments. The present experiments were under taken to investigate this issue, anatomically and functionally, with contemporary tools. We asked the following questions: 1) To what extent do the axons of individual RVLM neurons branch to innervate preganglionic neurons in disparate spinal levels (upper thoracic vs. lower thoracic/lumbar)? 2) Do RVLM neurons that project to lower thoracic/lumbar levels also send collateral connections that excite upper thoracic sympathetic outflows? 3) If so, do RVLM neurons that innervate both upper thoracic and lower thoracic/lumbar levels represent a sub-population of neurons that innervate functionally similar but anatomically distant targets as suggested by McAllen & Dampney (1990), or do they provide divergent drive to several functional classes of sympathetic outflow?

2 Methods

2.1 Ethical Approval

Experiments were approved by Macquarie University (Research Authority 2011-057) and Florey Institute of Neuroscience and Mental Health (Research Authority 13-032) Animal Ethics Committees and conformed to the Australian code for the care and use of animals for scientific purposes (2013), and Journal of Physiology and ARRIVE guidelines.

2.2 Anatomical tracing

Evidence for RVLM bulbospinal neurons that innervate multiple spinal segments was sought in experiments in which two replication-deficient retrograde viral vectors that expressed different fluorophores were each injected into the upper or lower thoracic spinal cord. Adult Sprague Dawley rats (Animal Resource Centre, Perth, Australia) were housed in 12 hour light-dark cycles in individually ventilated cages with *ad libitum* access to food and water. Data presented in the current paper were obtained from 10 male rats (222 – 380 g), with data rejected from a further 6 animals due to poor labelling. A further 13 male and female rats were used to optimise time course and vector targeting.

On the day of surgery animals were anaesthetised with ketamine and medetomidine (75 mg/kg i.p., Parnell Laboratories, Australia, and 0.75 mg/kg i.p., Pfizer Animal Health, Australia, respectively), treated with prophylactic analgesia (carprofen, 2.5 – 10 mg/kg s.c., Norbrook Pharmaceuticals, Australia) and antibiotics (cephazolin, 100 mg/kg i.m., Mayne Pharma, Australia), the fur on the back clipped, and the skin scrubbed with betadine. Anaesthesia was assessed by examining withdrawal of the hind paw in response to noxious pinch and was supplemented with ketamine (7.5 mg/kg i.p.) as required. Rats were positioned in a stereotaxic frame on a thermostatically controlled heated blanket and the T_2 and T_{10} spinal cord exposed by blunt dissection of the overlying muscles and separation of the spinous ligament (T_2) or laminectomy (T_{10}). Adjacent vertebrae were clamped for stability. Bilateral pressure injections of HSV-hCMV-GFP or HSV-hCMV-mCherry vectors (supplied at 3 x 10^8 IU/ml, Rachael Neve, McGovern Institute for Brain Research at MIT, USA) were made at the interomediolateral column (IML) using a glass pipette mounted on a manipulator. Injections were targeted 1 mm deep to the dorsal root entry, approximately 0.7 mm lateral to midline. Appropriate co-

ordinates were verified in initial experiments by addition of blue polystyrene beads to the injectate (1:10,000, Thermo Scientific, Australia, #09980508).

We first established that HSV-hCMV-GFP and HSV-hCMV-mCherry vectors result in equivalent retrograde transduction of medullary neurons. This was achieved by injecting a 1:1 mixture of HSV-hCMV-GFP and HSV-hCMV-mCherry at the T_2 IML (2 x 500 nl injections on each side of the spinal cord separated by 1 mm rostrocaudal) and examining the proportion of medullary neurons that expressed both reporters four days later (n = 2 animals).

In subsequent experiments HSV-hCMV-GFP was used to label T_2 -projecting neurons and HSV-hCMV-mCherry for T_{10}-projecting neurons. Two 500 nl injections of each vector were made bilaterally (i.e. a total of 2 µl of each vector). Injections were made over 5 – 10 minutes and pipettes left in place a further 5 minutes to minimise vector leak from the parenchyma.

After injections the spinal cord was irrigated with sterile saline and covered with Gelfoam. Skin incisions were closed with metal clips and anaesthesia reversed with atipamazole (1 mg/kg s.c., Pfizer Animal Health, Australia) and rats monitored closely until ambulatory. Rats were housed singly for 4-5 days after vector injections with frequent monitoring including daily weighing and behavioural assessment and additional analgesia as required.

2.3 Histology & immunohistochemistry

At the conclusion of experiments rats were euthanised with sodium pentobarbitone (>150 mg/kg, Lethabarb, Virbac, Australia) and transcardially perfused with 300 ml cold heparinized saline followed by 300 ml 4 % paraformaldehyde. The brain and thoracic spinal cord were removed, post-fixed overnight and the medulla blocked and cut into 50 µm coronal sections in a 1-in-4 series. For anatomy experiments sections were permeabilized in 0.2% Triton-100 (3 x 15 mins) then incubated with primary antibody (Sigma T1299 monoclonal mouse anti-tyrosine hydroxylase (TH: AB_477560), 1: 1000) for 48 hours in TPBS containing 2% bovine serum albumin. Sections were then washed (3 x 30 minutes) and incubated overnight in blocking buffer containing Alexa Fluor® 647-conjugated secondary antibody (Life Technologies A31571 polyclonal goat anti-mouse (AB_162542), 1:500). Sections were washed again in TPBS (3 x 15 minutes), mounted in order, and coverslipped with Dako mounting medium. No immunohistochemical processing was required to visualise GFP- or mCherry fluorescence. Brain sections that spanned the RVLM were imaged under epifluorescence (Zeiss AxioImager Z2 microscope, 10x/0.30 NA M27 objective, 0.645 µm pixel size).

In two cases rats were perfused with modified acrylamide-paraformaldehyde fixative solution and cleared using the CLARITY protocol (Tomer *et al.*, 2014). 48 hours after perfusion the fixative was polymerized and the brainstems cut into 1 mm thick coronal sections using a brain matrix. Sections were then incubated with SDS/borate buffer and passively cleared over several weeks before mounting in a custom imaging chamber filled with glycerol. CLARITY-processed brains were tile-imaged using a Leica TCS SP5X confocal microscope.

2.4 Functional Studies

In electrophysiology experiments, we examined whether photoactivation of RVLM neurons that project to the lower spinal cord also produced responses in functionally similar and functionally distinct sympathetic nerves that emerge from the upper cord. A schematic diagram presenting our overall hypothesis and experimental strategy is presented in Figure 4. Functional studies

were carried out in 44 male Sprague-Dawley rats (200-370 g) bred on-site at the Florey Institute. Animals were on a 12/12 light-dark cycle and had free access to food and water. Anaesthesia was induced with sodium pentobarbitone (60 mg/kg, i.p.) and maintained with 2-3% isoflurane in oxygen; the criterion for successful anaesthesia was areflexia to a strong pinch. Animals were treated with meloxicam (Ilium, 0.5 mg, i.m.) and atropine (Pfizer, 60 µg, i.m.) for analgesia and prevention of excessive tracheal secretion respectively, then transferred to a homeostatic heating blanket controlled via rectal temperature probe and maintained at 37 ± 1 °C.

The caudal-most rib was used as a landmark to identify the T_{13} vertebral segment. Overlying muscle was cleared from the T_{12}-L_1 vertebrae: the spinal level at which sympathetic preganglionic neurons which target hindlimb muscle vasoconstrictor neurons are primarily found (Sonnenschein & Weissman, 1978; Baron *et al.*, 1988). The T_{12} vertebra was clamped for mechanical stability, and a laminectomy was performed. A drop of lidocaine was placed on the spinal cord surface to prevent spinal locomotor reflexes and 250-300 nl of a canine adenoviral vector (CAV2-CMV-Cre, supplied at 2.5 x 10^{12} pp/ml, Eric Kramer, Plateforme de Vectorologie de Montpellier, France) was pressure injected into the left IML via a bevelled glass micropipette (diameter 20 µm) positioned just lateral to the posterior spinal vasculature and 0.5 mm ventral to the spinal surface. Injection volume was determined by visualization of the fluid level within the micropipette using a microscope fitted with a calibrated graticule. The micropipette was left in place for at least 2 minutes; 6 - 9 such injections were made per animal at intervals of approximately 0.5 mm in the rostrocaudal direction.

Animals were then secured in a stereotaxic frame tilted 10° nose-down and the dorsal aspect of the skull was exposed. A small craniotomy was drilled overlying the injection sites and a micropipette filled with AAV-EF1a-DIO-hChR2-mCherry (AAV serotype 2), supplied at 1×10^{13} vg/mL, Penn Vector Core, Pennsylvania, USA) was advanced into the region of the left RVLM (AP: 11.96, ML: -2.1, DV: -10.5). Nanoinjection (100-200 nl) was frequently associated with respiratory artefacts (tachypnoea or bradypnoea) indicating that injections were in the region of the ventrolateral medulla. After the initial injection, the micropipette was advanced rostrally at intervals of 0.2-0.3 mm until nanoinjection produced twitching of the whiskers, indicating proximity to the facial nucleus, an anatomical landmark for the rostral margin of the RVLM. Once 3 or 4 injections had been performed injections were repeated 0.3 mm more medially at the same antero-posterior coordinates. In total, 6-8 injections of 100-200 nl were made spanning the region 1.8-2.1 ML, 11.3-12.7 mm AP.

This intersectional approach enabled us to target those neurons with cell bodies in the region of the RVLM and whose axons project to the thoracolumbar spinal cord: only neurons that were exposed to viral vector at both the central and the spinal injection site would express ChR2.

Exposed tissue was irrigated with sterile saline, a piece of sterile Gelfoam (Pfizer, Australia) was placed over the exposed surface of the spinal cord, and incisions were closed in layers using silk thread. Anaesthesia was discontinued and animals closely attended until ambulatory. They were then monitored daily signs of spinal cord injury, pain or weight loss.

2.5 Electrophysiological recordings and optogenetic stimulation

11-50 days after vector injections, surgical anaesthesia was induced as described above. Animals were tracheostomised and artificially ventilated with 2% isoflurane in 100% oxygen.

The femoral artery and vein were cannulated for the monitoring of blood pressure and intravenous access respectively and rats placed in a stereotaxic frame. Paired recordings were undertaken in several combinations: forelimb and hindlimb muscle vasoconstrictor (MVC); cardiac sympathetic nerve (cSN) and lumbar sympathetic chain; cardiac sympathetic nerve and hindlimb MVC.

The left cardiac sympathetic nerve was isolated as described previously (Pracejus *et al.*, 2015). In brief, the head of the second rib was identified and cleared, taking care not to puncture the pleura. The head of the second (and often also the third) rib was removed and the peripheral portion retracted downwards: the stellate ganglion was accessed immediately underneath and was identified by its location and distinctive morphology (Korzina *et al.*, 2011). The cardiac sympathetic nerve(s) was identified by its trajectory from the lateral and/or caudal aspect of the stellate ganglion towards the heart and blunt-dissected free with fine forceps. It was then cut distally as it entered the pleura. It was led over a pair of fine silver wire electrodes under mineral oil and its activity was amplified and filtered (10-100 Hz high pass, 600-1000 Hz low pass: Neurolog, Welwyn Garden City, U.K.) and digitised at 5 kHz using a CED Power 1401 interface and Spike2 software (Cambridge Electronic Design, Cambridge, UK). An earth electrode was placed at the origin of the nerve from the stellate ganglion to minimise ECG contamination.

The lumbar sympathetic chain (LSN) on the left side was exposed via a retroperitoneal approach as described previously (Korim *et al.*, 2011), blunt-dissected and cut rostral to the L_3 ganglion. The left kidney was exposed and gently retracted. The lumbar sympathetic chain was blunt-dissected, isolated, and cut caudal to the L3 sympathetic ganglion. Its rostral end was placed across two silver wire electrodes and its activity recorded as described above.

Forelimb MVC nerve activity was recoded from the triceps branch of the ulnar nerve. The nerve was dissected from the triceps, cut distally, desheathed and placed over a small black plastic dissection platform under mineral oil. Filaments were split from its central end using watchmaker's forceps and a razor shard. Activity was recorded differentially between an active filament and a strand of connective tissue led over two fine silver wire electrodes. Hindlimb MVC activity was recorded from the gastrocnemius branch of the popliteal nerve using a similar approach. MVC spike activity was identified by its irregular ongoing activity, usually modulated by the cardiac cycle.

A fibreoptic probe connected to a 473 nm LASER (BL473T5-200: Shanghai Laser & Optics Century Co. Ltd.) was stereotactically placed immediately dorsal to the RVLM to stimulate Channelrhodopsin2 (ChR2)-expressing neurons (AP: 11.96 from bregma, ML -2.1, DV -10.5). Pulses of light (10-20 ms, 10 mW) were delivered at 1 or 2 Hz.

At the conclusion of 32 electrophysiology experiments, rats were perfusion-fixed as described above. The brain was removed, post-fixed overnight, and cut into 50 µm sections. Brainstem sections that spanned the RVLM were examined for mCherry fluorescence.

2.6 Statistical analysis

Identification and mapping of RVLM neurons with bifurcating axons

50 µm RVLM sections were aligned to the Waxholm volumetric rat brain atlas (Papp *et al.*, 2014) using the QuickNII affine registration tool (https://www.nitrc.org/projects/quicknii).

Labelled neurons lying in a triangle defined by the ventral midline surface, nucleus ambiguus, and medial border of the spinal trigeminal tract were manually annotated and classified based on the presence of GFP, mCherry, and/or TH immunoreactivity. The pixel co-ordinates of annotated neurons were transformed into Waxholm co-ordinates as previously described (Dempsey *et al.*, 2017).

Labelling exhibited some variability between animals: experiments in which retrograde labelling from T_2 or T_{10} was conspicuously absent were assumed to reflect off-target vector injections and were eliminated from analysis. Previous experiments using HSV vectors indicated that retrograde transduction of spinally projecting RVLM neurons was largely restricted to the ipsilateral side (Dempsey *et al.*, 2017) and therefore labelling on one side of the brainstem was considered independent to labelling on the other. Therefore, although data were collected from both right and left sides of the medulla, data were transformed and pooled such that all were plotted on the left side.

Only neurons that lay within the anatomical boundaries of the RVLM were included in analysis. The RVLM was defined using a 3D density map of TH-immunoreactive neurons that were retrogradely labelled with GFP or mCherry (n = 273); computed at a 1 voxel (39 μm) resolution using a parametric density mapping method (Burguet *et al.*, 2011; Burguet & Andrey, 2014) and with the smoothing parameter k set to 10. The boundary of the RVLM was defined as the isodensity surface that contained 85% of the TH+ bulbospinal neurons. The RVLM boundary iso-surface and the Cartesian co-ordinates of identified bulbospinal neurons were then imported into Imaris software (Version 8.1, Bitplane AG, Switzerland). Neurons falling within the RVLM were identified using an Imaris script (*'Spots split into surface objects'*, http://open.bitplane.com/tabid/235/Default.aspx?id=19) and tabulated, allowing elimination of neurons that fell outside of the RVLM. X, Y and Z co-ordinates from each replicate were plotted as mean ± SEM, grouped, and compared in Graphpad Prism 7.02 using 1-way ANOVA followed, if significant, by Tukey post-tests between groups. $P < 0.05$ was considered significant. The 3D spatial distributions of GFP-, mCherry- and double-labelled RVLM neurons were pooled over replicates and were assessed by extracting the 85% isodensity surfaces from the three corresponding density maps as described above. The proportion of bulbospinal neurons that expressed TH immunoreactivity was compared by Chi squared test.

Photoactivation of sympathetic nerves

Stimulus-triggered averages of rectified and smoothed (time constant = 10 ms) nerve activity were used to identify activation of post-ganglionic sympathetic nerves. At least 750 sweeps were averaged in each case. Time-locked peaks in SNA that exceeded the pre-stimulus amplitude by at least 2 standard deviations were interpreted as proof of optogenetic stimulation. Negative controls were obtained by repositioning the fibreoptic probe 3 mm dorsal to the RVLM and repeating the same procedure or by disconnecting it from the laser. The pre-stimulus mean and standard deviation (σ) were calculated using a period of 200 ms before laser stimulation. At the conclusion of electrophysiology recordings animals were perfusion-fixed. Brainstems were prepared for histology as described above and RVLM hChR2-mCherry expression was verified.

3 Results

3.1 Axon collateralization to upper and lower spinal segments by RVLM neurons: anatomical evidence

Spinal injections of recombinant herpes vectors drove robust labelling in the RVLM that was apparent within 24 hours and maximal after 4-5 days. Within the ventral medulla, spinally projecting neurons formed a continuous band that spanned the RVLM, rostral ventromedial medulla/gigantocellular reticular nucleus and midline *raphé pallidus, magnus* and *obscurus* nuclei (Figure 1A).

We first examined whether GFP- and mCherry-driving HSV variants drove equivalent reporter expression by co-injecting both at the T_2 spinal cord and examining the degree of reporter co-localisation in retrogradely transduced medullary neurons. Labelled neurons were counted in three sections each from two such experiments. The percentage of labelled neurons that contained both reporters was 81% and 91% (Figure 1B). This suggests that synaptic terminals within the vicinity of the injection site approached saturation, even when vectors were diluted by half, and that retrograde labelling of both was equally efficient.

We then examined whether colocalization of fluorophores could be observed when HSV variants were microinjected at different spinal segments (HSV-GFP at T_2, HSV-mCherry at T_{10} - Figure 2A-C). A similar pattern was seen in each experiment; of the 70 ± 8 retrogradely labelled RVLM neurons identified per side (eleven hemi-medullae from 6 animals), 21 ± 2 % contained both GFP and mCherry, 53 ± 3% s contained GFP only (corresponding to labelling from T_2), and 26 ± 3% contained mCherry only (corresponding to labelling from T_{10}). Double-labelled neurons were more likely to express TH than neurons single-labelled with GFP or mCherry (43% of double-labelled neurons contained TH compared to 24% of GFP- & 29% of mCherry-only neurons, Chi-square $P<0.00001$). Similarly, the ratio of double: single-labelled TH-positive neurons was higher than for TH-negative neurons (0.32 vs 0.18, Fisher's Exact $P<0.0001$). An incidental finding of the current study was the presence of double-labelled neurons in the rostral ventromedial medulla (RVMM), the midline raphé nuclei, and the C3 cell group, but the prevalence of spinal bifurcation in sympathetic premotor groups other than the RVLM was not systematically investigated.

The spatial distributions of RVLM neurons retrogradely labelled from T_2, T_{10}, or both spinal segments were plotted in 3D space and compared (Figure 2D & E, Figure 3). The distributions of all three groups overlapped substantially; however, density maps (Figure 3E) and statistical analysis of the Cartesian co-ordinates of labelled neurons (Figure 3F-H) indicate that neurons that innervate the upper spinal cord lie caudal and dorsal to neurons that innervate the lower spinal cord. Mean rostrocaudal Waxholm coordinates were 310.5 ± 0.5 voxels (GFP) versus 314.6 ± 0.7 (mCherry, Tukey $P<0.001$) and 313.8 ± 0.8 (GFP + mCherry, Tukey $P<0.01$, Figure 3G), corresponding to a mean difference of ~160 μm. Mean dorsoventral coordinates were 186.5 ± 0.4 (GFP) versus 184.3 ± 0.6 voxels (mCherry: Tukey $P<0.01$, Figure 3H), corresponding to a mean difference of 86 μm. There was no significant difference in the dorsoventral co-ordinates of double-labelled neurons (185.4 ± 0.5) compared to single-labelled neurons.

3.2 Axon collateralization to upper and lower spinal sympathetic outflows by RVLM neurons: functional evidence

Paired sympathetic nerve recordings were made in 39 rats that had previously received spinal injections of the retrogradely transported vector CAV-Cre and ipsilateral RVLM injections of a cre-dependent AAV that drives ChR2. In 13 of these animals we observed time-locked activation of one or more sympathetic nerves in response to light pulses delivered to the ipsilateral RVLM.

Histological sections from 32 rats (9 from experiments in which time-locked photoactivation of sympathetic nerves was observed; 23 in which it was not) were examined for mCherry fluorescence. mCherry-labelled RVLM neurons were always observed in experiments in which photostimulation evoked sympathetic responses and tended to be more sparse (14 rats) or absent (9 rats) in experiments during in which no responses were recorded. Labelled neurons from successful experiments were concentrated within the RVLM and, to a lesser extent, the RVMM, with occasional (<1 neuron per experiment) mCherry neurons in the raphé nuclei. No mCherry cells were seen in the C3 or NTS regions (Figures 4B & 5C).

We first studied collateralization of RVLM neurons that innervate anatomically distinct but functionally similar outflows by simultaneously recording MVC activity in the ipsilateral forelimb and hindlimb. Intermittent optogenetic stimulation of RVLM neurons that were retrogradely transduced from the lower spinal cord resulted in time-locked activation of forelimb SNA (4/4 animals), with co- activation of hindlimb SNA observed in 3/4 animals. In all cases detected peaks exceeded the background level of nerve activity by >4 σ (Figure 5A, left panel) and were abolished by withdrawal of the optrode by 3 mm (Figure 5C). In some cases smaller stimulus-locked responses were still apparent when stimulation was delivered 2 mm dorsal to the RVLM (Figure 6D). Such residual activity may reflect the dorsal axonal trajectories of these neurons or their collateralised innervation of the NTS (Lipski *et al.*, 1995; Stornetta *et al.*, 2016). Peaks in forelimb SNA had response latencies between 125-211 ms, while hindlimb SNA peaked at 195-288 ms. Responses were typically single-peaked, although in one animal a double-peaked response was observed in forelimb MVC activity (peaks at 125 ms and 211 ms, Figure 5B). These findings indicate that some RVLM neurons with axonal projections to the lower spinal cord (presumably innervating MVC preganglionic neurons) also provide collateral excitation to upper thoracic preganglionic neurons that supply forelimb MVC.

We then investigated whether evidence of functional collateralization of RVLM neurons is observable in non-MVC sympathetic outflows. For this, we again used injection of CAV-cre in the lower spinal cord combined with injection of AAV-DIO-ChR2 in the medulla to control ChR2 expression in the RVLM. We recorded activity from the cardiac sympathetic nerve at the same time as either the hindlimb MVC (n = 4, Figure 6A) or L2 lumbar sympathetic chain (n = 4, Figure 6B). Intermittent optogenetic stimulation of the RVLM produced pulse-locked activation of the cardiac sympathetic nerve with amplitudes exceeding those observed during the pre-stimulus period by 5σ in all 8 animals tested. Peak cardiac sympathetic nerve response latencies fell between 53-158 ms. A double peak (63 and 112 ms) was seen in one animal (Figure 6C). Stimulus-locked activation of hindlimb MVC was observed in 3/4 experiments (peak latencies: 180-313 ms), one of which featured a double peak (latencies: 203 ms and 313 ms, Figure 6D). On average, peaks in hindlimb MVC activity occurred 121 ± 10.4 ms after those of the cardiac nerve. Stimulus-locked activation of the lumbar sympathetic outflow was observed in 4/4

experiments (peak latencies: 152-229 ms). On average, peaks in lumbar sympathetic activity occurred 76.5 ± 4.6 ms after those of the cardiac nerve.

As reported by Abbott *et al.* (2009), laser-evoked SNA responses were sometimes followed by post-burst inhibition that lasted 100 – 200 ms; periods of reduced nerve activity that exceeded σ by 4-6 fold were apparent in forelimb MVC (2/4 animals), cardiac SN (2/8 animals), lumbar SN (1/4 animals); hindlimb MVC (1/6 animals). In addition, 2 recordings of hindlimb MVC showed significant laser-evoked inhibition of SNA that was not preceded by activation (5-6σ, latency 253 & 275 ms).

4 Discussion

The current study addresses the organizational principle/s by which RVLM neurons regulate sympathetic nerve activity. As discussed in the introduction, it is clear from the literature that RVLM neurons are not a homogeneous population. The unsettled questions are the extent to which they are anatomically and functionally selective and to what extent individual RVLM neurons make widespread projections with more generalized sympathetic actions.

Using more refined tools than were previously available, we found that a substantial minority of RVLM neurons send collaterals to diverse spinal segments. Using replication-deficient retrograde viral tracers injected at upper or lower thoracic spinal segments we found that, in addition to neurons that expressed only green or red fluorescent reporters (indicating projections to the T_2 or T_{10} thoracic cord respectively) 21% of spinally projecting RVLM neurons were found to contain both.

Next, we used an intersectional approach in which RVLM neurons that project to the lower spinal cord were selectively transduced to express ChR2. Responses to light stimulation of the RVLM were recorded in sympathetic nerves that emerged from both upper and lower spinal cord segments. Intermittent stimulation of retrogradely transduced neurons evoked activity in both upper and lower sympathetic outflows, including both functionally similar (forelimb and hindlimb MVC) and functionally dissimilar sympathetic nerves (cardiac and hindlimb MVC/lumbar sympathetic chain). Electrophysiological responses recorded in rostral outputs occurred at shorter latencies than simultaneously recorded responses recorded in caudal sympathetic outputs. As expected, the latencies of responses evoked in forelimb and cardiac sympathetic nerves were consistent with the latencies of responses evoked by optogenetic or electrical stimulation of RVLM neurons (Morrison & Reis, 1991; Abbott *et al.*, 2009) and with the latencies of antidromic responses to spinal cord stimulation recorded in functionally identified sympathetic premotor neurons (Brown & Guyenet, 1985; Verberne *et al.*, 1999). Although we believe these results are best explained by activation of RVLM neurons with axon collaterals within the spinal cord, it is worth touching upon other possibilities.

First, there is the chance that sympathetic outputs from the upper spinal cord were excited not via collateral branches within the spinal cord, but rather by collateral activation of premotor neurons within the RVLM (or other sympathetic premotor nuclei). Anatomical evidence suggests that this is plausible: C1 neurons, including those with spinal axons, give rise to collateral branches that terminate within the ipsi- and contralateral RVLM (Lipski *et al.*, 1995;

McMullan & Pilowsky, 2012; Turner *et al.*, 2013; Stornetta *et al.*, 2016), and to a lesser extent the A5, C3, and raphe pallidus (Stornetta *et al.*, 2016). Furthermore, ultrastructural analysis and trans-synaptic viral tracing confirms synaptic connectivity between C1 neurons and neighbouring RVLM neurons (both C1 and non-C1) (Milner *et al.*, 1987; Agassandian *et al.*, 2012; Dempsey *et al.*, 2017). It could therefore be argued that activation of proximal sympathetic outflows in the current study is due to excitation of untransduced bulbospinal neurons by their ChR2-expressing neighbours. However, functional studies have yielded no evidence of detectable coupling between bulbospinal neurons *in vivo* (McAllen *et al.*, 2001) or *in vitro* (L Bou Farah & S McMullan, unpublished observation), and therefore synaptic connectivity between adjacent RVLM neurons seems an unlikely explanation for our electrophysiological results.

An alternative explanation is that a small portion of preganglionic neurons in the lower thoracic cord that are activated by RVLM stimulation could perhaps project rostrally to innervate sympathetic post-ganglionic neurons that innervate the forelimb or heart. Similarly, ChR2-expressing RVLM neurons may target interneurons in the lower cord that innervate preganglionic neurons in the upper thoracic cord. Although it does seem that some preganglionic neurons innervate very distant targets, and can in some cases innervate more than one sympathetic ganglion (Jansen *et al.*, 1993; Pyner & Coote, 1994), the proportion of those that do so is small, even in instances where the ganglia in question are anatomically close and are supplied by neurons with a largely overlapping spinal distribution (Jansen *et al.*, 1993). Moreover, the responses evoked in forelimb or cardiac sympathetic outputs occurred at shorter latencies than those recorded in lumbar or hindlimb outputs in every case in the current study, indicating that responses in proximal outputs were not secondary to a relay in the lower cord.

In the absence of evidence for functional coupling between adjacent medullary bulbospinal neurons or collateralisation of sympathetic preganglionic neurons, we conclude that optogenetic activation of premotor sympathetic neurons innervating both upper and lower spinal segments represents the simplest explanation for our observations. Anatomical data from the current study unequivocally demonstrate that such a population of neurons exists. These collateralized axonal projections constitute an entirely plausible anatomical substrate for our electrophysiological observations.

4.1 Topographical considerations

Our findings are consistent with a study that found dual-labelling of RVLM neurons following application of two distinct retrograde trans-synaptic viruses applied to the stellate ganglion and the adrenal gland of the rat (Jansen *et al.*, 1995). The presence of sympathetic premotor neurons in the RVLM (and elsewhere) that were infected by both agents was taken as evidence that these cells innervate both targets. However, the polysynaptic nature of these viruses, in combination with uncertainty regarding the degree of connectivity between local RVLM sympathetic premotor neurons, makes the interpretation of this study difficult (Morrison, 2001).

The results of our anatomical study also share some features with a previous survey in the cat, which used fast blue and Fluoro-Ruby to retrogradely label RVLM neurons from T_4 and T_{10} (Gowen *et al.*, 2012). Though these investigators described a smaller proportion of double-labelled RVLM bulbospinal neurons (<10%), they found (as did we) that double-labelling was more common in C1 neurons than in non-C1 neurons. This finding is consistent with the view espoused by Guyenet and colleagues that activation of C1 neurons may underlie the global

sympathoexcitation evoked by physiological stressors (Guyenet *et al.*, 2013) (although this does not necessarily translate to a more significant role for C1 neurons compared to non-C1 neurons in the generation of baseline vasomotor tone, as we have previously argued (Burke *et al.*, 2011)). Our results are in stark contrast to those of Tucker and Saper (1985), who found that less than 1% of spinally projecting neurons were double-labelled when using a combination of fast blue, nuclear yellow or diamidino yellow tracers in the rat. Although differences in the spinal segments chosen for tracer injections could contribute to this discrepancy, it seems more likely that differences in the uptake efficiency sensitivities of the tracers used may underlie the higher incidence of double-labelling observed in the current study. Here, co-injection of both HSV vectors at the *same* spinal level led to colocalization of fluorophores in over 80% of neurons. As Tucker and Saper (1985) found only 20-30% of spinally projecting neurons were double-labelled under the same conditions, the true extent of collateralization when those tracers were injected at different spinal levels would have been greatly underestimated.

From a technical perspective, the anatomical component of the current study extends the connectomic approach that we recently developed for the analysis, mapping and visualisation of anatomical datasets (Dempsey *et al.*, 2017). Specifically, we have now incorporated a density-mapping technique that plots the anatomical boundaries of a brain structure based on the distribution of the individual neurons that define it. This allowed us to probabilistically define the RVLM based on objective criteria (the distribution of bulbospinal TH-expressing cells) and to limit our analysis to neurons that fell within this region. The boundary of the RVLM as we have defined it here extends more medially than that described by the widely referred to anatomical atlas of Paxinos and Watson (2006) and more closely resembles a functional map constructed by the examination of cardiovascular responses to medullary glutamate microinjections in the anaesthetised rat (Goodchild & Moon, 2009). Our approach may be useful to other investigators who wish to define the anatomical boundaries of regions of interest using cell-specific criteria (such as neurochemical phenotype, functional profile, or connectivity). This approach revealed previously unrecognised topographical differences in the distribution of RVLM bulbospinal neurons that project to different spinal cord segments: neurons labelled from the upper spinal cord were located caudal to bifurcating neurons or neurons labelled from the lower spinal cord exclusively.

4.2 Limitations

A key assumption of our anatomical study is that tracer injected in the upper spinal cord gained entry to neurons that form synaptic terminals in the vicinity of the injection site without labelling fibres of passage. Whereas labelling of fibres of passage is essentially unavoidable when using traditional chemical tracers (Chen & Aston-Jones, 1995; Vercelli *et al.*, 2000), this limitation does not appear to apply to HSV vectors, which rely on interactions between the viral envelope glycoprotein complex and cell surface receptors to gain intracellular access (reviewed by Frampton *et al.*, 2005; Sathiyamoorthy *et al.*, 2017). In neurons, the synaptic adhesion molecule nectin-1 is the critical mediator of HSV cell entry and infection (Geraghty *et al.*, 1998). As nectin-1 is predominantly expressed on presynaptic terminals (Mizoguchi *et al.*, 2002) but is not normally expressed in fibre tracts (Castellanos *et al.*, 2013), we conclude that HSV-mediated reporter expression likely reflects vector uptake at synaptic terminals.

This is likely not the case for the CAV-Cre used in functional experiments, which seems to be able to retrogradely access neurons via axons of passage as well as synaptic terminals (Schwarz

et al., 2015). However, our basic conclusion is unaffected: because vector injections were made only in the lower spinal cord: if any passing axons were labelled, they would have been in transit to lumbar or lower levels. Thus, optogenetic activation of upper thoracic sympathetic outflows can confidently be attributed to collateral branches of axons that project to the thoracolumbar cord.

It should be noted that the methodology used in physiology experiments permits detection of neurons with both upper thoracic and thoracolumbar projections, it does not permit us to definitively identify the functional class of these neurons. We are unable to distinguish between neurons which innervate every studied output (e.g. the vasculature of the forelimb muscle, the heart and the vasculature of the hindlimb muscle) and neurons that innervate only a subset of these targets. Though anatomical and functional studies have demonstrated that the thoracolumbar junction is a locus of preganglionic sympathetic neurons that target muscle vascular beds in the hindlimb (Sonnenschein & Weissman, 1978; Baron *et al.*, 1988), neurons with other targets are also present. Preganglionic sympathetic neurons at this level also innervate the inferior and, to a lesser extent, the superior mesenteric ganglion (Strack *et al.*, 1988) and also target the pelvic viscera and associated vasculature (Sonnenschein & Weissman, 1978; Kaleczyc, 1998; Hsieh *et al.*, 2000). Thus, though our anatomical data indicate that collateralization of sympathetic premotor neurons is widespread, our electrophysiological observations do not extend further than the pairs of outflows we studied.

Finally, the stimulus-triggered averaging used to detect laser-triggered responses in sympathetic outputs warrants consideration. This commonly used technique has the benefit of high sensitivity, enabling the pooling of thousands of responses to repeated stimuli in order to distinguish small excitatory or inhibitory events from background noise. However, the amplitude of these responses is greatly influenced by the number of active fibres within the nerve, but also by factors which are impossible to control and likely to vary from experiment to experiment: these include the number of inactive or damaged fibres, the amount of fat or connective tissue in the nerve sheath, the hydration of the nerve, and the properties of the recording electrodes. Therefore, this method cannot be readily used to compare the amplitudes of responses recorded in different animals: it should be viewed as a sensitive tool for the detection of collateralisation, but of limited use for its quantification. The comparison of responses that were simultaneously recorded from rostral and caudal sympathetic outputs would be similarly limited. Responses recorded from rostral outputs (e.g. hindlimb muscle vasoconstrictor) in response to optogenetic stimulation are presumably due to activation of RVLM neurons that project to the caudal spinal cord but that possess axon collaterals that innervate the rostral spinal cord. However, since responses recorded from caudal outputs (e.g. hindlimb muscle vasoconstrictor) are driven by RVLM neurons with terminals at the same spinal level to which the retrograde viral vector was applied (the caudal spinal cord), responses recorded from these outputs are presumably driven by collateralized and non-collateralized neurons alike.

4.3 Functional significance

Our anatomical and functional data indicate that the RVLM possesses a population of bulbospinal 'command neurons' that dictate the behaviour of multiple sympathetic outputs as suggested by (Barman & Gebber, 1985); who observed that a majority of barosensitive bulbospinal RVLM neurons in the cat could be antidromically activated by electrical stimulation

at multiple spinal levels, and concluded that some RVLM neurons "exert widespread excitatory effects on sympathetic outflow".

These may correspond to either or both of two functional arrangements: (a) widely collateralised axon projections that innervate the same functional class of preganglionic neuron at multiple spinal levels (e.g. MVC nerves throughout the body) – 'functionally specific'; or (b) neurons that simultaneously drive outflows of different functional class – 'generalist'.

We and others have long argued that many, perhaps most, RVLM neurons have a specialized, selective connection to a single class of sympathetic preganglionic neuron. This is supported by studies in which careful nanoinjection of glutamate into selected regions of the cat RVLM could have effects that were largely restricted to individual functional classes of sympathetic outflow (Dampney & McAllen, 1988; McAllen & Dampney, 1990; McAllen & May, 1994). Calculations from such experiments were used to support a quantitative argument that the majority of RVLM neurons were functionally specified to drive one class of outflow (McAllen & May, 1994). In rats, similar investigations have produced less conclusive results. In this species, nanoinjection of glutamate into the RVLM almost always produces simultaneous activation of functionally diverse sympathetic outflows (Beluli & Weaver, 1991a, b; Mueller *et al.*, 2011). Proponents of functional specificity in RVLM neurons cite the small size of the rat RVLM and the limitations of glutamate nanoinjection as an investigatory tool to explain this result, and point out that the extent to which sympathetic nerve activity is activated in outflows of different functional type in response to nanoinjecton of glutamate into the RVLM is variable.

The results of the current study suggest otherwise: optogenetic stimulation of the RVLM produced simultaneous activation not only of sympathetic outflows to both forelimb and hindlimb vascular beds, but also to the heart. The simultaneous activation of forelimb and hindlimb MVC nerves is in harmony with the notion that the rat RVLM contains neurons which comprise functionally specific subtypes. However, the activation of the cardiac nerve does *not* support this idea. On the contrary, this result suggests that the collateralised neurons studied here (or some subset of them) are generalist in nature. Therefore, while the present findings not challenge the existence of functionally specific RVLM neurons, we must conclude that a population of generalist RVLM neurons does exist.

Some key questions remain. Do neurons with divergent axons represent a single functional class of 'general' sympathetic premotor neurons, or does functional specialisation exist within this population such that particular groups of branching RVLM premotor neurons connect to functional subsets of preganglionic neurons at different levels of the spinal cord? A key function of RVLM bulbospinal neurons is to provide the tonic drive that maintains vasomotor tone and supports blood pressure: are 'generalist' RVLM neurons part of that tonically active population, or are they recruited under emergency conditions to drive more widespread activation of sympathetic target organs? What is the overall incidence of branching within the premotor population; how many spinal segments are targeted by these neurons? The current study only sampled RVLM neurons that innervate the T_2 and T_{10} spinal segments; many other potential pairings exist but were not examined. Such information would clarify whether the relatively high incidence of dual innervation of the segments examined here reflects some peculiarity about these targets, or whether generalised innervation of preganglionic neurons represents a widespread organisational scheme through which RVLM sympathetic premotor neurons exert influence on sympathetic nerve activity.

5 Competing interests.

The authors declare no competing interests.

6 Author Contributions

Experiments were carried out at the Florey Institute of Neuroscience and Mental Health and at Macquarie University. DGSF, NP, RMM, AKG, PB, BD, JFRP, AEP and SM conceived and designed the experiments. DGSF and NP conducted and analysed the functional experiments. AT, BD and PB conducted the anatomical experiments. BD, PA & SM analysed the anatomical experiments. JB and PA designed and implemented the spatial distribution analysis tools. All authors contributed to interpretation of the data. DGSF, SM, NP and RMM drafted the article. All authors contributed to critical revision of this article. All authors approved the final version of the manuscript and qualify for authorship. All those who qualify for authorship have been listed.

7 Funding

This work was funded by the Australian Research Council (DP130104661, DP120100920) and the Faculty of Medicine, University of Melbourne, and Macquarie University postgraduate scholarships (BD & PB). JFRP is funded by the British Heart Foundation (RG/12/6/29670). AEP is a Wellcome Trust Senior Clinical fellow (gr088373). We also acknowledge the support of the Victorian Government through the Operational Infrastructure Scheme. The Institut Jean-Pierre Bourgin benefits from the support of the LabEx Saclay Plant Sciences-SPS (ANR-10-LABX-0040-SPS).

8 Acknowledgements

The authors acknowledge the kind assistance of Mr David Trevaks and Gregory Thomas. HSV vectors kindly supplied by Rachael Neve, McGovern Viral Core Facility. CAV vectors kindly supplied by Eric Kremer from the Montpellier Gene Vector Core at IGGM.

9 References

Abbott SB, Stornetta RL, Socolovsky CS, West GH & Guyenet PG. (2009). Photostimulation of channelrhodopsin-2 expressing ventrolateral medullary neurons increases sympathetic nerve activity and blood pressure in rats. *J Physiol* **587,** 5613-5631.

Agassandian K, Shan Z, Raizada M, Sved AF & Card JP. (2012). C1 catecholamine neurons form local circuit synaptic connections within the rostroventrolateral medulla of rat. *Neuroscience* **227,** 247-259.

Barman SM & Gebber GL. (1985). Axonal projection patterns of ventrolateral medullospinal sympathoexcitatory neurons. *J Neurophysiol* **53,** 1551-1566.

Baron R, Janig W & Kollmann W. (1988). Sympathetic and afferent somata projecting in hindlimb nerves and the anatomical organization of the lumbar sympathetic nervous system of the rat. *J Comp Neurol* **275,** 460-468.

Beluli DJ & Weaver LC. (1991a). Areas of rostral medulla providing tonic control of renal and splenic nerves. *Am J Physiol* **261,** H1687-1692.

Beluli DJ & Weaver LC. (1991b). Differential control of renal and splenic nerves without medullary topography. *Am J Physiol* **260,** H1072-1079.

Brown DL & Guyenet PG. (1985). Electrophysiological study of cardiovascular neurons in the rostral ventrolateral medulla in rats. *Circ Res* **56,** 359-369.

Burguet J & Andrey P. (2014). Statistical comparison of spatial point patterns in biological imaging. *PLoS One* **9,** e87759.

Burguet J, Maurin Y & Andrey P. (2011). A method for modeling and visualizing the three-dimensional organization of neuron populations from replicated data: Properties, implementation and illustration. *Pattern Recognition Letters* **32,** 1894-1901.

Burke PG, Neale J, Korim WS, McMullan S & Goodchild AK. (2011). Patterning of somatosympathetic reflexes reveals nonuniform organization of presympathetic drive from C1 and non-C1 RVLM neurons. *Am J Physiol Regul Integr Comp Physiol* **301,** R1112-1122.

Cannon WB. (1915). *Bodily Changes in Pain, Hunger, Fear and Rage*. D. Appleton & Company, New York, NY.

Cao WH, Madden CJ & Morrison SF. (2010). Inhibition of brown adipose tissue thermogenesis by neurons in the ventrolateral medulla and in the nucleus tractus solitarius. *Am J Physiol Regul Integr Comp Physiol* **299,** R277-290.

Castellanos KJ, Gagyi E, Kormos B, Valyi-Nagy K, Voros A, Shukla D, Horvath S, Slavin KV & Valyi-Nagy T. (2013). Increased axonal expression of nectin-1 in multiple sclerosis plaques. *Neurol Sci* **34,** 465-469.

Chen S & Aston-Jones G. (1995). Evidence that cholera toxin B subunit (CTb) can be avidly taken up and transported by fibers of passage. *Brain Res* **674,** 107-111.

Dampney RA. (1994). Functional organization of central pathways regulating the cardiovascular system. *Physiological Reviews* **74,** 323-364.

Dampney RA & McAllen RM. (1988). Differential control of sympathetic fibres supplying hindlimb skin and muscle by subretrofacial neurones in the cat. *J Physiol* **395,** 41-56.

Dempsey B, Le S, Turner A, Bokiniec P, Ramadas R, Bjaalie JG, Menuet C, Neve R, Allen AM, Goodchild AK & McMullan S. (2017). Mapping and Analysis of the Connectome of Sympathetic Premotor Neurons in the Rostral Ventrolateral Medulla of the Rat Using a Volumetric Brain Atlas. *Front Neural Circuits* **11,** 9.

Frampton AR, Jr., Goins WF, Nakano K, Burton EA & Glorioso JC. (2005). HSV trafficking and development of gene therapy vectors with applications in the nervous system. *Gene Ther* **12,** 891-901.

Geraghty RJ, Krummenacher C, Cohen GH, Eisenberg RJ & Spear PG. (1998). Entry of alphaherpesviruses mediated by poliovirus receptor-related protein 1 and poliovirus receptor. *Science* **280,** 1618-1620.

Goodchild AK & Moon EA. (2009). Maps of cardiovascular and respiratory regions of rat ventral medulla: focus on the caudal medulla. *J Chem Neuroanat* **38,** 209-221.

Gowen MF, Ogburn SW, Suzuki T, Sugiyama Y, Cotter LA & Yates BJ. (2012). Collateralization of projections from the rostral ventrolateral medulla to the rostral and caudal thoracic spinal cord in felines. *Exp Brain Res* **220,** 121-133.

Guyenet PG. (2006). The sympathetic control of blood pressure. *Nat Rev Neurosci* **7,** 335-346.

Guyenet PG, Stornetta RL, Bochorishvili G, Depuy SD, Burke PG & Abbott SB. (2013). C1 neurons: the body's EMTs. *Am J Physiol Regul Integr Comp Physiol* **305,** R187-204.

Hsieh NK, Liu JC & Chen HI. (2000). Localization of sympathetic postganglionic neurons innervating mesenteric artery and vein in rats. *J Auton Nerv Syst* **80,** 1-7.

Janig W & McLachlan EM. (1992). Characteristics of function-specific pathways in the sympathetic nervous system. *Trends Neurosci* **15,** 475-481.

Jansen ASP, Farwell DG & Loewy AD. (1993). Specificity of pseudorabies virus as a retrograde marker of sympathetic preganglionic neurons: implications for transneuronal labeling studies. *Brain Research* **617,** 103-112.

Jansen ASP, Van Nguyen X, Karpitskiy V, Mettenleiter TC & Loewy AD. (1995). Central command neurons of the sympathetic nervous system: Basis of the fight-or-flight response. *Science* **270,** 644-646.

Kaleczyc J. (1998). Origin and neurochemical characteristics of nerve fibres supplying the mammalian vas deferens. *Microsc Res Tech* **42,** 409-422.

Korim WS, Bou Farah L, McMullan S & Verberne AJ. (2014). Orexinergic activation of medullary premotor neurons modulates the adrenal sympathoexcitation to hypothalamic glucoprivation. *Diabetes* **63,** 1895-1906.

Korim WS, Llewellyn-Smith IJ & Verberne AJ. (2016). Activation of Medulla-Projecting Perifornical Neurons Modulates the Adrenal Sympathetic Response to Hypoglycemia: Involvement of Orexin Type 2 (OX2-R) Receptors. *Endocrinology* **157,** 810-819.

Korim WS, McMullan S, Cravo SL & Pilowsky PM. (2011). Asymmetrical changes in lumbar sympathetic nerve activity following stimulation of the sciatic nerve in rat. *Brain Res* **1391,** 60-70.

Korzina MB, Korobkin AA, Vasilieva OA & Masliukov PM. (2011). Morphological Characteristics of the Stellate Ganglion in White Rats. *Neuroscience and behavioral physiology* **41,** 436-439.

Lipski J, Kanjhan R, Kruszewska B & Smith M. (1995). Barosensitive neurons in the rostral ventrolateral medulla of the rat in vivo: morphological properties and relationship to C1 adrenergic neurons. *Neuroscience* **69,** 601-618.

McAllen RM. (1986). Action and specificity of ventral medullary vasopressor neurones in the cat. *Neuroscience* **18,** 51-59.

McAllen RM. (1987). Central respiratory modulation of subretrofacial bulbospinal neurones in the cat. *J Physiol* **388,** 533-545.

McAllen RM & Dampney RA. (1990). Vasomotor neurons in the rostral ventrolateral medulla are organized topographically with respect to type of vascular bed but not body region. *Neurosci Lett* **110,** 91-96.

McAllen RM & May CN. (1994). Differential drives from rostral ventrolateral medullary neurons to three identified sympathetic outflows. *Am J Physiol* **267,** R935-944.

McAllen RM, Trevaks D & Allen AM. (2001). Analysis of firing correlations between sympathetic premotor neuron pairs in anesthetized cats. *J Neurophysiol* **85,** 1697-1708.

McMullan S, Pathmanandavel K, Pilowsky PM & Goodchild AK. (2008). Somatic nerve stimulation evokes qualitatively different somatosympathetic responses in the cervical and splanchnic sympathetic nerves in the rat. *Brain Res* **1217,** 139-147.

McMullan S & Pilowsky PM. (2012). Sympathetic premotor neurones project to and are influenced by neurones in the contralateral rostral ventrolateral medulla of the rat in vivo. *Brain Res* **1439,** 34-43.

Milner TA, Pickel VM, Park DH, Joh TH & Reis DJ. (1987). Phenylethanolamine N-methyltransferase-containing neurons in the rostral ventrolateral medulla of the rat. I. Normal ultrastructure. *Brain Res* **411,** 28-45.

Miyawaki T, Pilowsky P, Sun QJ, Minson J, Suzuki S, Arnolda L, Llewellyn-Smith I & Chalmers J. (1995). Central inspiration increases barosensitivity of neurons in rat rostral ventrolateral medulla. *American Journal of Physiology* **268,** R909-918.

Mizoguchi A, Nakanishi H, Kimura K, Matsubara K, Ozaki-Kuroda K, Katata T, Honda T, Kiyohara Y, Heo K, Higashi M, Tsutsumi T, Sonoda S, Ide C & Takai Y. (2002). Nectin: an adhesion molecule involved in formation of synapses. *J Cell Biol* **156,** 555-565.

Moraes DJ, da Silva MP, Bonagamba LG, Mecawi AS, Zoccal DB, Antunes-Rodrigues J, Varanda WA & Machado BH. (2013). Electrophysiological properties of rostral ventrolateral medulla presympathetic neurons modulated by the respiratory network in rats. *J Neurosci* **33,** 19223-19237.

Morrison SF. (2001). Differential control of sympathetic outflow. *American Journal Of PhysiologyRegulatory, Integrative And Comparative Physiology* **281,** R683-R698.

Morrison SF & Cao WH. (2000). Different adrenal sympathetic preganglionic neurons regulate epinephrine and norepinephrine secretion. *American journal of physiology Regulatory, integrative and comparative physiology* **279,** R1763-R1775.

Morrison SF & Reis DJ. (1991). Responses of sympathetic preganglionic neurons to rostral ventrolateral medullary stimulation. *Am J Physiol* **261,** R1247-1256.

Mueller PJ, Mischel NA & Scislo TJ. (2011). Differential activation of adrenal, renal, and lumbar sympathetic nerves following stimulation of the rostral ventrolateral medulla of the Rat.

American Journal of Physiology - Regulatory Integrative and Comparative Physiology **300,** R1230-R1240.

Papp EA, Leergaard TB, Calabrese E, Johnson GA & Bjaalie JG. (2014). Waxholm Space atlas of the Sprague Dawley rat brain. *Neuroimage* **97,** 374-386.

Paxinos G & Watson C. (2006). *The Rat Brain in Stereotaxic Coordinates*. Academic Press.

Pracejus NH, Farmer DG & McAllen RM. (2015). Segmental origins of cardiac sympathetic nerve activity in rats. *Auton Neurosci* **187,** 45-49.

Pyner S & Coote JH. (1994). Evidence that sympathetic preganglionic neurones are arranged in target-specific columns in the thoracic spinal cord of the rat. *J Comp Neurol* **342,** 15-22.

Sathiyamoorthy K, Chen J, Longnecker R & Jardetzky TS. (2017). The COMPLEXity in herpesvirus entry. *Curr Opin Virol* **24,** 97-104.

Schwarz LA, Miyamichi K, Gao XJ, Beier KT, Weissbourd B, DeLoach KE, Ren J, Ibanes S, Malenka RC, Kremer EJ & Luo L. (2015). Viral-genetic tracing of the input-output organization of a central noradrenaline circuit. *Nature* **524,** 88-92.

Sonnenschein RR & Weissman ML. (1978). Sympathetic vasomotor outflows to hindlimb muscles of the cat. *Am J Physiol* **235,** H482-487.

Stalbovskiy AO, Briant LJ, Paton JF & Pickering AE. (2014). Mapping the cellular electrophysiology of rat sympathetic preganglionic neurones to their roles in cardiorespiratory reflex integration: a whole cell recording study in situ. *J Physiol* **592,** 2215-2236.

Stornetta RL, Inglis MA, Viar KE & Guyenet PG. (2016). Afferent and efferent connections of C1 cells with spinal cord or hypothalamic projections in mice. *Brain structure & function* **221,** 4027-4044.

Strack AM, Sawyer WB, Marubio LM & Loewy AD. (1988). Spinal origin of sympathetic preganglionic neurons in the rat. *Brain Res* **455,** 187-191.

Tomer R, Ye L, Hsueh B & Deisseroth K. (2014). Advanced CLARITY for rapid and high-resolution imaging of intact tissues. *Nature Protocols* **9,** 1682-1697.

Tucker DC & Saper CB. (1985). Specificity of spinal projections from hypothalamic and brainstem areas which innervate sympathetic preganglionic neurons. *Brain Res* **360,** 159-164.

Turner A, Kumar N, Farnham M, Lung M, Pilowsky P & McMullan S. (2013). Rostroventrolateral medulla neurons with commissural projections provide input to sympathetic premotor neurons: anatomical and functional evidence. *Eur J Neurosci* **38,** 2504-2515.

Verberne AJ & Sartor DM. (2010). Rostroventrolateral medullary neurons modulate glucose homeostasis in the rat. *Am J Physiol Endocrinol Metab* **299,** E802-807.

Verberne AJ, Stornetta RL & Guyenet PG. (1999). Properties of C1 and other ventrolateral medullary neurones with hypothalamic projections in the rat. *Journal of Physiology* **517 (Pt 2),** 477-494.

Vercelli A, Repici M, Garbossa D & Grimaldi A. (2000). Recent techniques for tracing pathways in the central nervous system of developing and adult mammals. *Brain Res Bull* **51,** 11-28.

10 Figure Legends

Figure 1 A. Reporter expression in the ventral medulla following microinjection of HSV-hCMV-GFP at the T_2 spinal cord. 930 µm thick optical stack from a CLARITY-cleared brainstem block; insert shows corresponding atlas plate at Bregma -12.12, Paxinos and Watson (2006). A'. Enlarged view of region denoted by orange box in Panel A. B Control experiment: extensive colocalisation of reporter expression following co-injection of retrograde HSV variants at the T_2 spinal cord. GFP and mCherry channels are merged such that double-labelled neurons appear white. Individual channel images shown in Bi & Bii. na: nucleus ambiguus. Panel C shows injection sites in the upper (left) and lower (right) thoracic spinal cord marked by fluorescent beads.

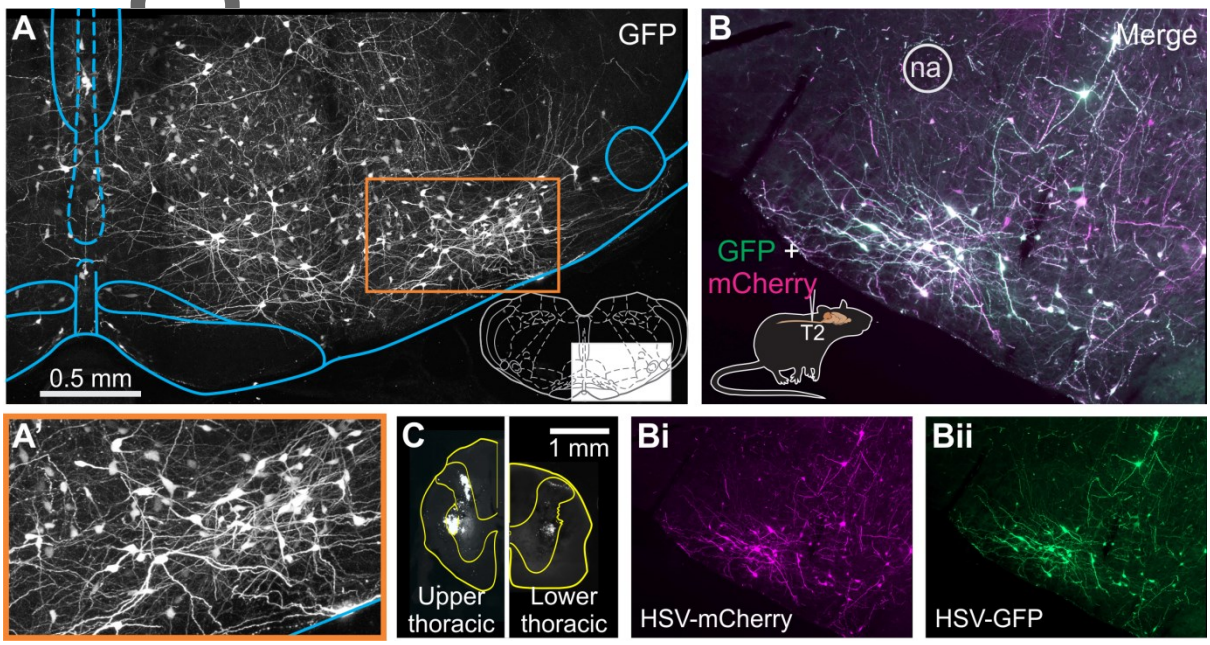

Figure 2 Injection of retrograde HSV variants at different levels of the spinal cord results in reporter colocalization in the RVLM. A. Epifluoresence image of a 50 µm brainstem section at the level of the RVLM showing distribution of reporters and tyrosine hydroxylase (TH). B. Experimental scheme: HSV-GFP and HSV-mCherry were microinjected at the T_2 and T_{10} spinal cord respectively. C. Confocal image of boxed region in panel A: double-labelled neurons containing both GFP and mCherry made up about 20% of the bulbospinal population and included TH-immunoreactive C1 neurons (Ci, arrow) and TH-negative non-C1 neurons (Cii, arrow). Co-ordinates of bulbospinal neurons were transformed into Waxholm space (D shows data corresponding to panel A aligned onto Waxholm reference dataset; E shows 1561 bulbospinal neurons from 11 replicates projected into 3D Waxholm segmentation model. sp5: spinal trigeminal tract; py: pyramidal tract; na: nucleus ambiguus.

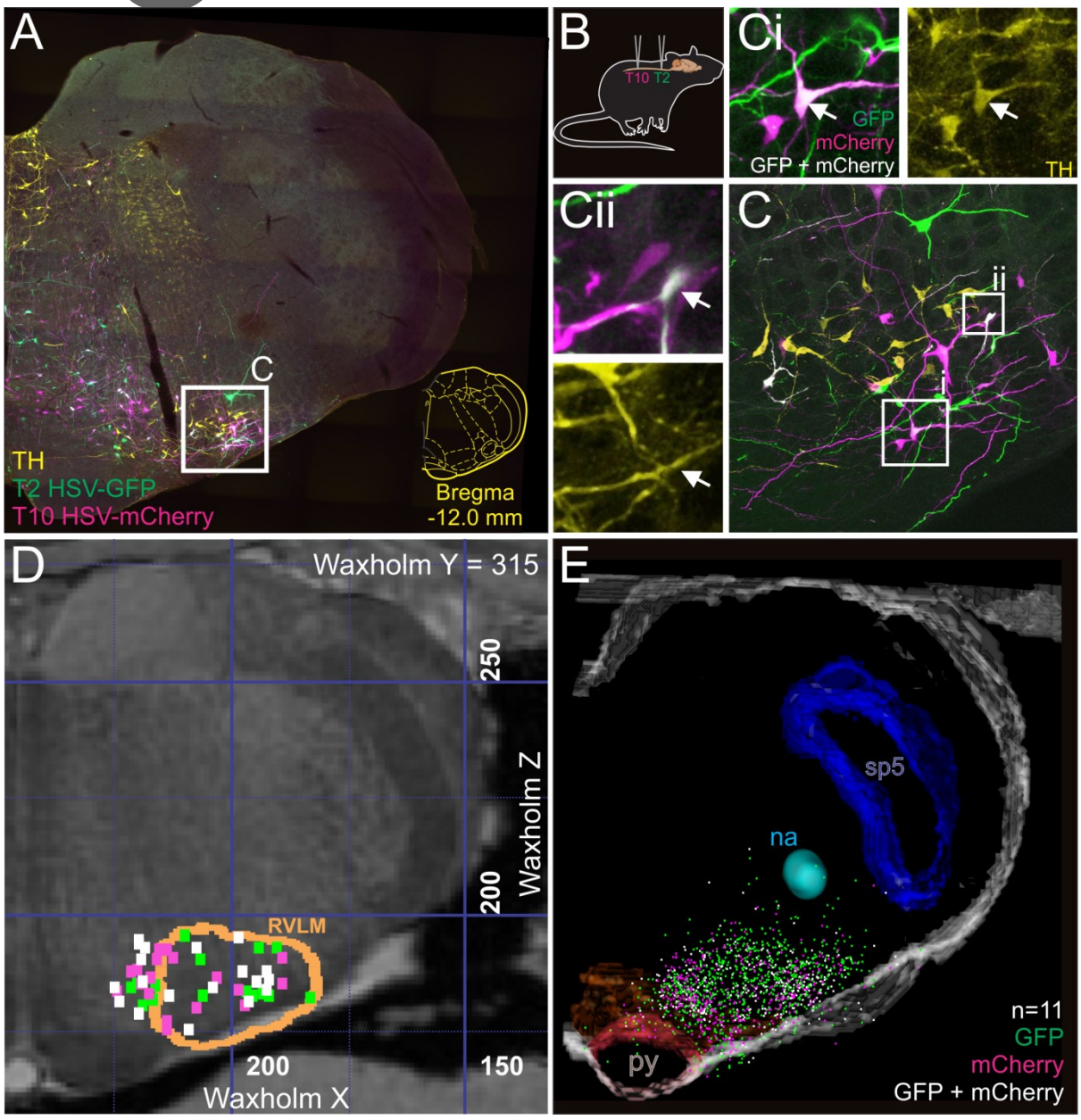

*Figure 3 Comparison of distributions of RVLM neurons projecting to the upper or lower spinal cord, or to both. A. Ventral view of Waxholm ventral medulla; anatomical landmarks are pyramidal tract (Py), facial nucleus (VII), inferior olive (Inf Ol) and nucleus ambiguus (na). B. Enlarged view of boxed region indicated in panel A showing distribution of 273 bulbospinal TH-immunoreactive neurons which were used to define the boundaries of the RVLM (green). C. Positions of spinally projecting neurons; neurons that fell outside of the RVLM boundary defined in B were excluded from analysis (D). E. Density maps showing 85% boundaries of GFP (green), mCherry (magenta) and double-labelled (white) RVLM neurons. F-H: mean mediolateral (F), rostrocaudal (G) and dorsoventral (H) coordinates of GFP, mCherry and double-labelled neurons. Each point shows the mean ± SEM of neurons from one replicate. **: P<0.01, ***: P<0.001*

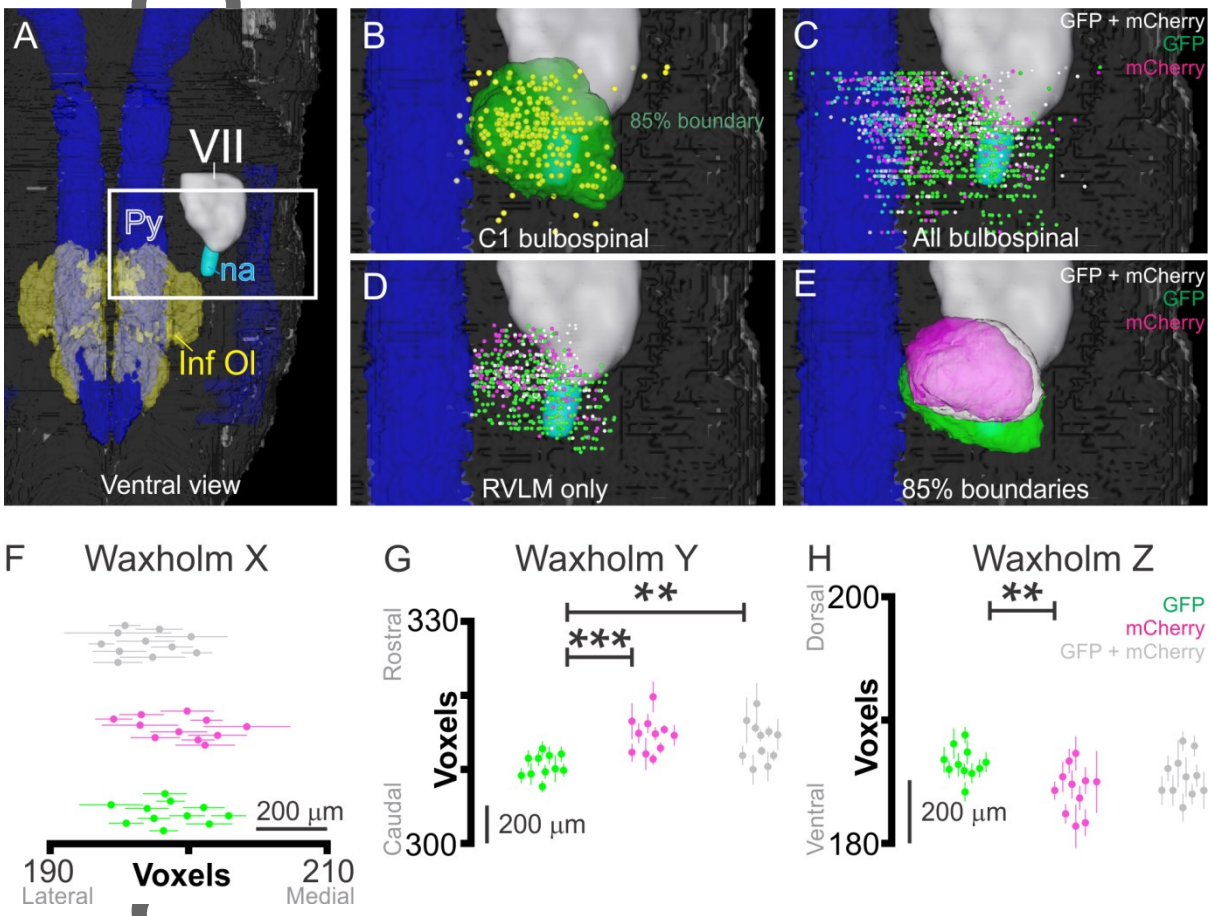

Figure 4 Conceptual overview of physiological experiments to test for the presence of collateralized RVLM 'command neurons'. Panel (A) depicts the intersectional optogenetic strategy. Panel (B) shows representative ChR2-mCherry expression in the RVLM in a successful experiment (scale bar = 100 µm). The relative position of the image is indicated in the camera lucida drawing underneath. Panels C, D and E depict different possible anatomical and functional organizations of collateralized RVLM neurons as described in panel and the expected result of electrophysiology experiments in each case. RVLM: rostral ventrolateral medulla; SNA: sympathetic nerve activity; SPN: sympathetic preganglionic neuron.

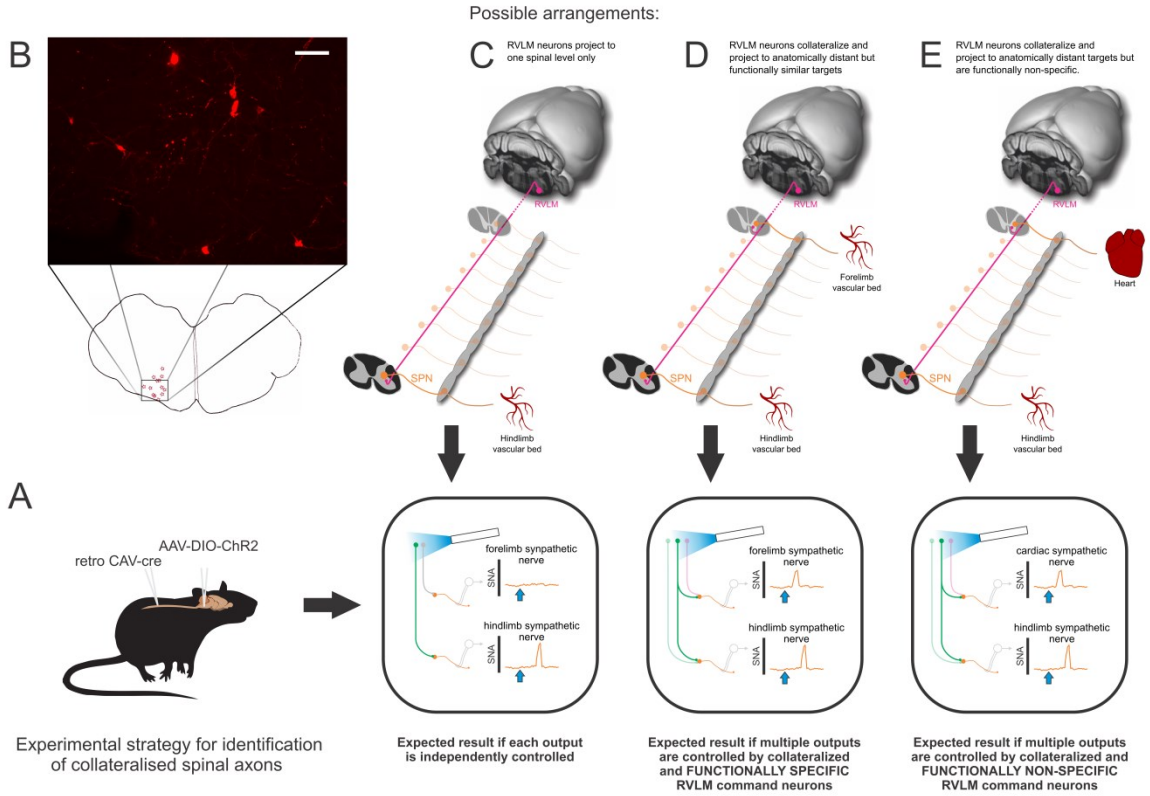

Figure 5. Collateralised pre-sympathetic neurons provide innervation of anatomically distant targets of similar functional type. Examples of stimulus-triggered averages of sympathetic nerve activity. Dotted lines indicate upper and lower control limits. A: Left panels depict averages of forelimb and hindlimb SNA triggered by light stimulation activation of the RVLM region (473 nm, 10 mW, 20 ms pulse width, 1 Hz; 1501 sweeps averaged). Right panels depict averaged nerve responses following withdrawal of the fibreoptic probe by 3 mm (control limits: ±6 σ, n = 1468 sweeps). B: The same average of forelimb SNA depicting a double peak in response to laser activation. After moving the fibreoptic probe 0.3 mm medially, the second peak is no longer present (control limits: ± 4σ, 900 sweeps averaged). C: Composite drawing showing the location of mCherry-positive neurons identified in sections that spanned the rostrocaudal extent of the RVLM in the experiment depicted above. SNA: sympathetic nerve activity.

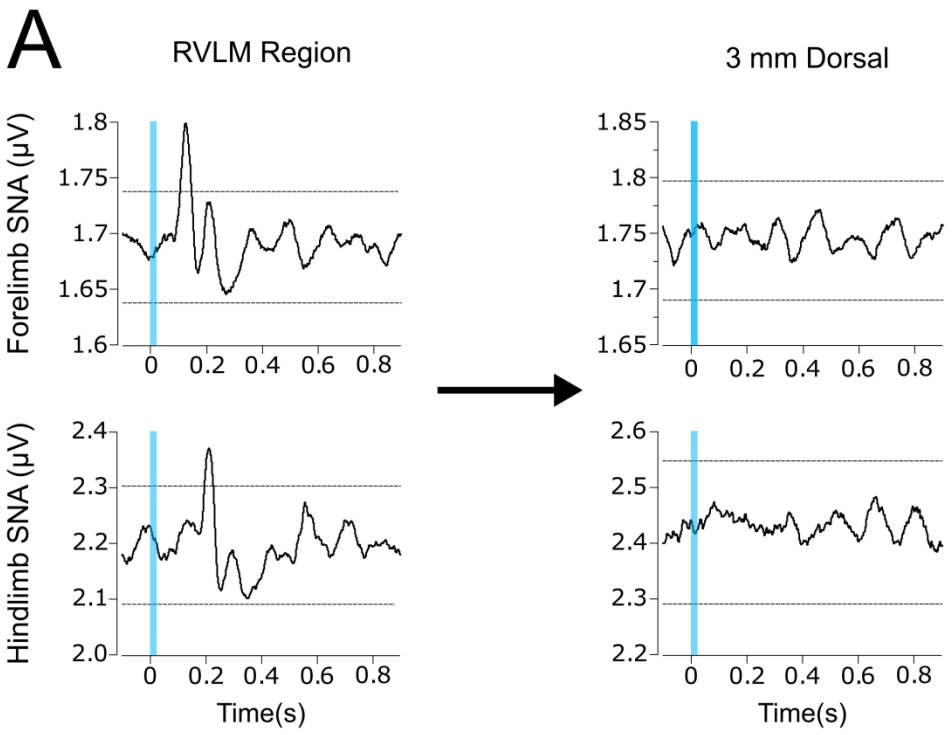

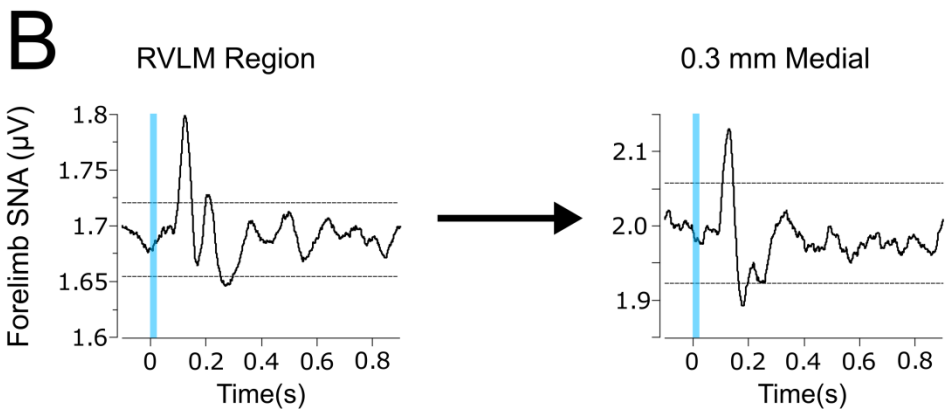

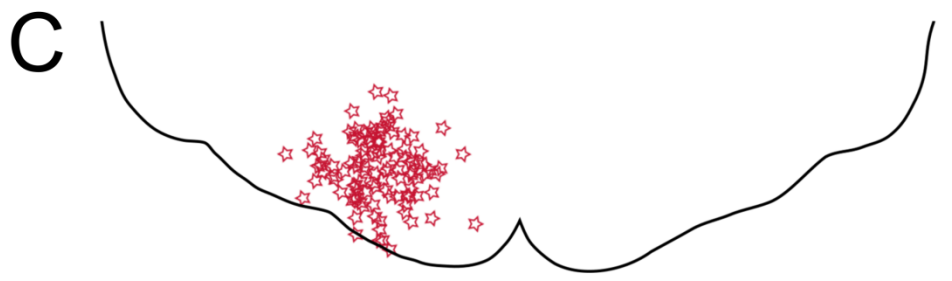

Figure 6. *Collateralised pre-sympathetic neurons innervate anatomically distant pre-ganglionic targets of dissimilar functional type. Examples of event-triggered averages of sympathetic nerve activity evoked by laser-stimulation of the RVLM region (473nm, 10mW, 20ms pulse width, 1-2Hz). Dotted lines indicate upper and lower control limits. A: Averages of light-evoked cardiac and hindlimb SNA (control limits: ± 6σ; 2493 sweeps averaged). B: Averages of light-evoked cardiac and lumbar SNA (control limits: ± 6σ; 3638 sweeps averaged). C: Average of light-evoked cardiac SNA: note the presence of two peaks (latencies of 63 ms and 112 ms; control limits: ± 6σ; 1075 sweeps averaged) and the period of inhibition which follows/. D: Average of light-evoked hindlimb MVC SNA evoked by flashing the RVLM region (left panel); note the presence of two peaks (latencies of 120ms and 203 ms; control limits: ± 6σ; 1080 sweeps averaged). On withdrawing the fibre-optic probe by 2mm dorsally (right panel), the faster peak still protrudes above the upper control limit (latency = 122 ms; control limits ± 6σ; 1080 sweeps averaged while the slower peak does not), suggesting that these two peaks arise due to stimulation of neurons at different topographical locations. SNA: sympathetic nerve activity.*

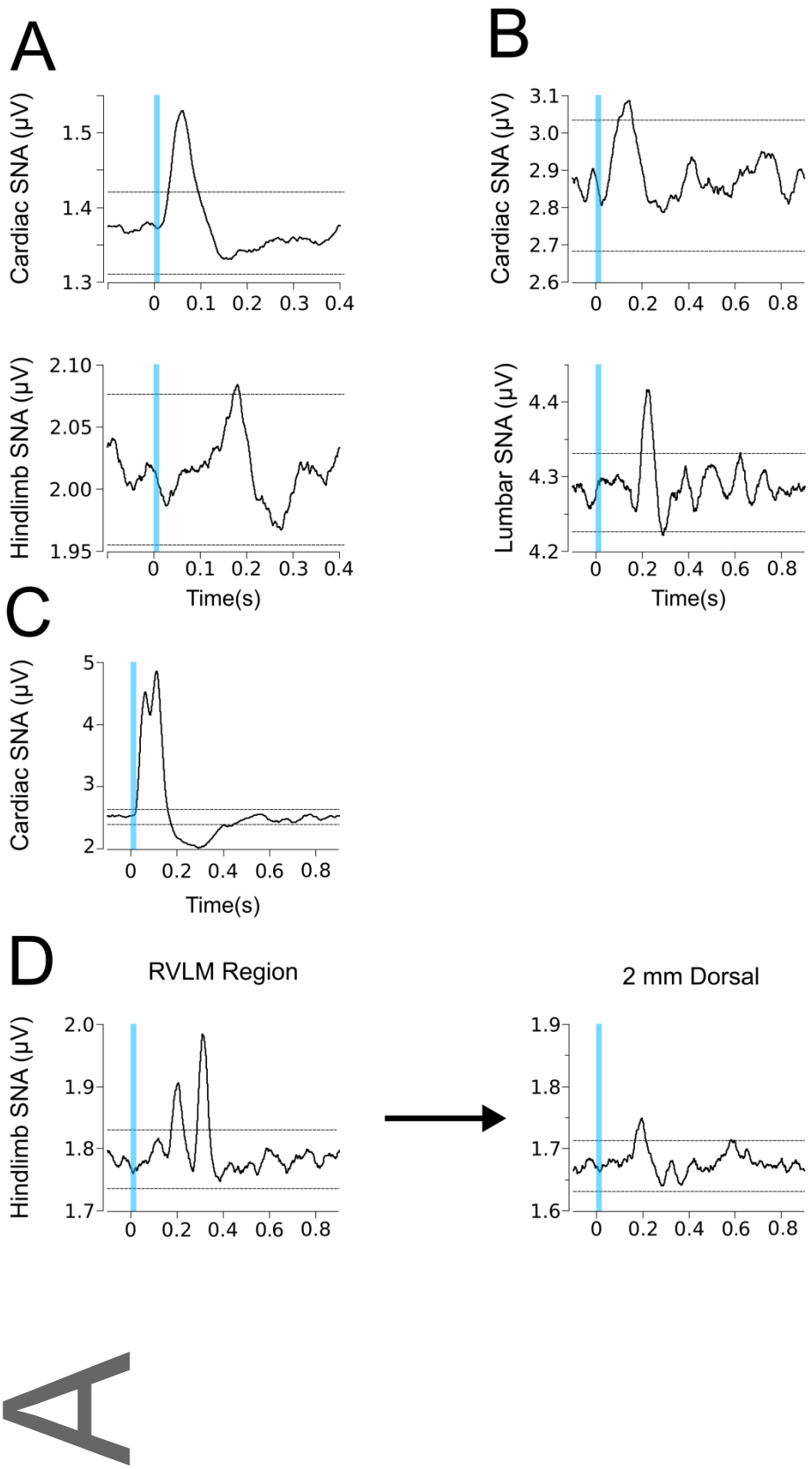

David Farmer is a Scottish/Australian neurophysiologist based in Melbourne, Australia. He is interested in the neural control of homeostasis (the cardiovascular system in particular) and has a longstanding (for his age) interest in the cough reflex.

Natasha Pracejus is a German/Australian neurophysiologist based in Melbourne, Australia. She completed her PhD at the Florey Institute of Neuroscience and Mental Health in 2017 and has since begun a post-doc at the Ion Channels and Human Diseases Laboratory, working with Praxis Precision Medicines on finding treatments for epilepsy and depression.